



# Bistable Dynamics Underlying Excitability of Ion Homeostasis in Neuron Models

Niklas Hübel<sup>1</sup>, Ekehard Schöll<sup>1</sup>, Markus A. Dahlem<sup>2\*</sup>

<sup>1</sup> Department of Theoretical Physics, Technische Universität Berlin, Berlin, Germany, <sup>2</sup> Department of Physics, Humboldt Universität zu Berlin, Berlin, Germany

## Abstract

When neurons fire action potentials, dissipation of free energy is usually not directly considered, because the change in free energy is often negligible compared to the immense reservoir stored in neural transmembrane ion gradients and the long-term energy requirements are met through chemical energy, i.e., metabolism. However, these gradients can temporarily nearly vanish in neurological diseases, such as migraine and stroke, and in traumatic brain injury from concussions to severe injuries. We study biophysical neuron models based on the Hodgkin–Huxley (HH) formalism extended to include time-dependent ion concentrations inside and outside the cell and metabolic energy-driven pumps. We reveal the basic mechanism of a state of free energy–starvation (FES) with bifurcation analyses showing that ion dynamics is for a large range of pump rates bistable without contact to an ion bath. This is interpreted as a threshold reduction of a new fundamental mechanism of *ionic excitability* that causes a long-lasting but transient FES as observed in pathological states. We can in particular conclude that a coupling of extracellular ion concentrations to a large glial–vascular bath can take a role as an inhibitory mechanism crucial in ion homeostasis, while the  $\text{Na}^+/\text{K}^+$  pumps alone are insufficient to recover from FES. Our results provide the missing link between the HH formalism and activator–inhibitor models that have been successfully used for modeling migraine phenotypes, and therefore will allow us to validate the hypothesis that migraine symptoms are explained by disturbed function in ion channel subunits,  $\text{Na}^+/\text{K}^+$  pumps, and other proteins that regulate ion homeostasis.

**Citation:** Hübel N, Schöll E, Dahlem MA (2014) Bistable Dynamics Underlying Excitability of Ion Homeostasis in Neuron Models. *PLoS Comput Biol* 10(5): e1003551. doi:10.1371/journal.pcbi.1003551

**Editor:** Lyle J. Graham, Université Paris Descartes, Centre National de la Recherche Scientifique, France

**Received:** October 8, 2013; **Accepted:** February 21, 2014; **Published:** May 1, 2014

**Copyright:** © 2014 Hübel et al. This is an open-access article distributed under the terms of the Creative Commons Attribution License, which permits unrestricted use, distribution, and reproduction in any medium, provided the original author and source are credited.

**Funding:** This work was supported by the Bundesministerium für Bildung und Forschung (BMBF 01GQ1001B, 01GQ1109) within the Bernstein Center of Computational Neuroscience Berlin. The funders had no role in study design, data collection and analysis, decision to publish, or preparation of the manuscript.

**Competing Interests:** The authors have declared that no competing interests exist.

\* E-mail: dahlem@physik.hu-berlin.de

## Introduction

The Hodgkin–Huxley (HH) model is one of the most successful models in mathematical biology [1]. This formalism, i.e., a HH-type model, describes voltage changes across cell membranes that result in excitability. Not only neurons are excitable cells, also myocytes, pancreatic  $\beta$ -cells, and even a plant cell (*Chara corallina*) exhibit excitable dynamics [2–4]. The dynamic range of phenomena includes single action potentials (spikes), periodic spiking, and bursting (slow modulation of spiking). For example, in pancreatic  $\beta$ -cells bursting is induced by a calcium current [4,5]. A more complete treatment of this phenomenon, however, also requires the inclusion of  $\text{Na}^+/\text{K}^+$  pumps [6]. The dynamics of ion pumps and ion concentrations is also crucial for cardiac rhythms (periodic beat-to-beat variations) and higher-order rhythms in the ischemic ventricular muscle [7–9].

In the literature such augmented HH-type models are also called second-generation HH models [10]. In the context of certain pathologies of the brain, whose fundamental dynamic structure we study here, we prefer the simpler name ‘ion-based’ models. This indicates that ion concentrations are major dynamical, that is, time-dependent variables. Their dynamical role in neuron models goes beyond merely modulating spiking activity. Ion dynamics can lead to a completely new type of *ionic excitability* and bistability, that is, the phenomena of so-called

‘spreading depolarizations’ and ‘anoxic depolarization’, respectively. (Spreading depolarizations are also called ‘spreading depression’ and we will use both names interchangeably in this paper.) These depolarized states of neurons are related to migraine, stroke, brain injury, and brain death, that is, to pathologies of the brain in which a transient or permanent break-down of the transmembrane potential occurs [11,12]. Another even more characteristic property of this ‘twilight state close to death’ [13] are the nearly completely flat transmembrane ion gradients. The almost complete break-down of both membrane potential and—due to reduced ion gradients—Nernst potentials together cause a nearly complete release of the Gibbs free energy, that is, the thermodynamic potential that measures the energy available to the neurons for normal functioning. We hence refer to this state as a state of free energy–starvation (FES). We want to stress that such phenomena require the broader thermodynamical perspective, because it goes beyond the HH description in terms equivalent electrical circuits in membrane physiology (see discussion).

The object of this study is to clarify quantitatively the detailed ion-based mechanisms, in particular the time-dependent potentials, leading to this condition. In fact, early ion-based models have been introduced in a different context to describe excitable myocytes and pancreatic  $\beta$ -cells with variable ion concentrations [14–16]. Neuronal ion-based models have been used to study

## Author Summary

Theoretical neuroscience complements experimental and clinical neuroscience. Simulations and analytical insights help to interpret data and guide our principal understanding of the nervous systems in both health and disease. The Hodgkin–Huxley–formulation of action potentials is certainly one of the most successful models in mathematical biology. It describes an essential part of cell-to-cell communication in the brain. This model was in various ways extended to also describe when the brain's normal performance fails, such as in migraine hallucinations and acute stroke. However, the fundamental mechanism of these extensions remained poorly understood. We study the structure of biophysical neuron models that starve from their 'free' energy, that is, the energy that can directly be converted to do work. Although neurons still have access to chemical energy, which needs to be converted by the metabolism to obtain free energy, their free energy-starvation can be more stable than expected, explaining pathological conditions in migraine and stroke.

spreading depolarizations (SD) [17–22] and anoxic depolarizations [21]. In these phenomenological studies the types of ion dynamics related to the pathologies have been reproduced, but not investigated in a bifurcation analysis. Hence the fundamental phase space structure of these high-dimensional models that underlies the ionic excitability characteristic of SD remains poorly understood. Furthermore, neuronal ion-based models have been used to study seizure activity [23,24] and spontaneous spiking patterns in myelinated axons with injury-like membrane damaging conditions (e.g., caused by concussions) [25,26]. In these models, the phase space structure was investigated, however, only with respect to the modulating effect of ion concentrations on the fast spiking dynamics (seizure activity, injuries), and with respect to spiking node-to-node transmission fidelity (myelinated axons).

In this paper we present bifurcation analyses of several minimal biophysical ion-based models that reveal bistability of extremely different ion configurations—physiological conditions vs. free energy-starvation—for a large range of pump rates. In related models certain bistabilities have been explored before. For example, Fröhlich et al. [27–29] found coexistence of quiescence and bursting for certain fixed extracellular potassium concentrations and also bistability of a physiological and a strongly depolarized membrane state in a slow-fast analysis of calcium gated channels. Bistability of similar fixed points has also been found for the variation of extracellular potassium [30] or, similarly, the potassium Nernst potential [31]. Also the effect of pump strength variation has been explored under fixed FES conditions [32]. In this paper, however, we do not treat slow variables as parameters and show bistability of fast dynamics, but instead we address the stability of ion concentrations themselves, which are subject to extremely slow dynamics. This allows us to find bistability of extremely different ion distributions, a feature that distinguishes these two states from the polarized and depolarized states studied in the afore mentioned work. A study that also had significantly different ion distributions was done by Cressman et al [33], however, the seizure-like phenomena discussed in their work are quite different—though clinically related—from those presented in this paper.

Because of the occurrence of ion state bistability we conjecture that our model describes a threshold reduction of a mechanism

that leads to ionic excitability in form of spreading depolarizations. In other words, we conclude that an important inhibitory mechanism to describe ion homeostasis such as glial buffering or diffusive regulation of extracellular ion concentrations plays a crucial role in ion homeostasis and the  $\text{Na}^+/\text{K}^+$  pumps alone are insufficient to recover from free energy-starved states. We show that when the extracellular  $\text{K}^+$  concentration is regulated by linearly coupling it to an infinite bath, the bistable system changes to an excitable system, which we call ionic excitability. The effect of turning off glial buffering and diffusion has been discussed in more detailed ion-based models [27,29] before, but has not been related to the fundamental phase space structure of the system. Our conclusions have been validated by demonstrating the robustness of the results in a large variety of minimal ion-based models, which all consistently show this insufficiency of  $\text{Na}^+/\text{K}^+$  pumps, and also in a very detailed membrane model that has been used intensively for computational studies of spreading depolarizations and seizure-like activity [17,34].

## Model

### Hodgkin–Huxley (HH) model and reductions

A simple ion-based neuron model can be obtained as a natural extension of the Hodgkin–Huxley (HH) model [1]. We list the basic equations of HH that we used for the sake of completeness, and also comment on two often used model reductions of which one must be modified for our study. Furthermore leak currents are specified, which is necessary for the extension towards ion-based modeling.

In the HH model, single neuron dynamics is described in terms of an electrically active membrane carrying an electric potential  $V$ , and the three gating variables  $n$ ,  $m$  and  $h$  that render the system excitable. Ion species included are sodium, potassium, and an unspecified ion carrying a leak current, which can be attributed to chloride in our extended model. The rate equations read [1]:

$$\frac{dV}{dt} = -\frac{1}{C_m}(I_{\text{Na}^+} + I_{\text{K}^+} + I_{\text{Cl}^-} - I_{\text{app}}), \quad (1)$$

$$\frac{dn}{dt} = \frac{n_\infty - n}{\tau_n}, \quad (2)$$

$$\frac{dh}{dt} = \frac{h_\infty - h}{\tau_h}, \quad (3)$$

$$\frac{dm}{dt} = \frac{m_\infty - m}{\tau_m}. \quad (4)$$

The top equation is simply Kirchhoff's current law for a membrane with capacitance  $C_m$  and membrane potential  $V$ .  $I_{\text{app}}$  is an externally applied current that may, for example, initiate voltage spikes. The gating variables  $n$ ,  $h$ , and  $m$  are the potassium activator, sodium inactivator, and sodium activator, respectively. Their dynamics is defined by their voltage-dependent asymptotic values  $x_\infty$  and relaxation times  $\tau_x$  ( $x = n, m, h$ ). These are given by

$$x_\infty = \frac{\alpha_x}{\alpha_x + \beta_x} \quad \text{and}$$

$$\tau_x = \frac{1}{\phi(\alpha_x + \beta_x)} \quad \text{for } x = n, m \text{ and } h.$$

Here  $\phi$  is a common timescale parameter, and the Hodgkin–Huxley exponential functions are

$$\alpha_m = \frac{0.1(V + 30)}{1 - \exp(-(V + 30)/10)}, \quad (5)$$

$$\beta_m = 4 \exp(-(V + 55)/18), \quad (6)$$

$$\alpha_n = \frac{0.01(V + 34)}{1 - \exp(-(V + 34)/10)}, \quad (7)$$

$$\beta_n = 0.125 \exp(-(V + 44)/80), \quad (8)$$

$$\alpha_h = 0.07 \exp(-(V + 44)/20), \quad (9)$$

$$\beta_h = \frac{1}{1 + \exp(-0.1(V + 14))}. \quad (10)$$

The individual ion currents read

$$I_{Na^+} = (g_{Na}^l + g_{Na}^g n^3 h) \cdot (V - E_{Na}), \quad (11)$$

$$I_{K^+} = (g_K^l + g_K^g n^4) \cdot (V - E_K), \quad (12)$$

$$I_{Cl^-} = g_{Cl}^l \cdot (V - E_{Cl}), \quad (13)$$

with  $g_{ion}^{l/g}$  denoting leak and gated conductances. In fact, Hodgkin and Huxley set up their model with an unspecified leak current and non-leaking sodium and potassium channels. As long as ion dynamics is not considered this is mathematically equivalent to specifying the leak current as being partially sodium, potassium and chloride, but it is physically inconsistent because the reversal potentials for the ions differ. In an ion-based approach, however, the main task of the ion pumps under physiological conditions is to compensate for sodium and potassium leak currents (see next section) while gated currents are extremely small in the equilibrium. So at this point leak currents for all ion species are important.

The Nernst potentials  $E_{ion}$  are given in terms of the ion concentrations  $[ion]$  in the intracellular space (ICS) and the extracellular space (ECS) denoted by subscripts  $i$  and  $e$ , respectively:

$$E_{ion} = \frac{26.64}{z_{ion}} \ln([ion]_e/[ion]_i), \quad (14)$$

for  $ion = K, Na$ , and  $Cl$  and  $z_{ion}$  is the ion valence. All model parameters are listed in Table 1. The units chosen are those typically used and appropriate for the order of magnitude of the

**Table 1.** Parameters for Hodgkin–Huxley model.

Name	Value & unit	Description
$C_m$	1 $\mu\text{F}/\text{cm}^2$	membrane capacitance
$\phi$	3/msec	gating timescale parameter
$g_{Na}^l$	0.0175 mS/cm <sup>2</sup>	sodium leak conductance
$g_{Na}^g$	100 mS/cm <sup>2</sup>	max. gated sodium conductance
$g_K^l$	0.05 mS/cm <sup>2</sup>	potassium leak conductance
$g_K^g$	40 mS/cm <sup>2</sup>	max. gated potassium conductance
$g_{Cl}^l$	0.05 mS/cm <sup>2</sup>	chloride leak conductance
$Na_i$	27 mMol/l	ECS sodium concentration
$Na_e$	120 mMol/l	ICS sodium concentration
$K_i$	130.99 mMol/l	ECS potassium concentration
$K_e$	4 mMol/l	ICS potassium concentration
$Cl_i$	9.66 mMol/l	ECS chloride concentration
$Cl_e$	124 mMol/l	ICS chloride concentration
$E_{Na}$	39.74 mV	sodium Nernst potential
$E_K$	-92.94 mV	potassium Nernst potential
$E_{Cl}$	-68 mV	chloride Nernst potential

doi:10.1371/journal.pcbi.1003551.t001

respective quantities. Time is measured in msec, potentials in mV, and ion concentrations in mMol/l. The units for conductance densities imply that ionic and pump current densities are in  $\mu\text{A}/\text{cm}^2$ . For better readability we omit the square brackets on the ion concentrations and simply write  $K_{i/e}$ ,  $Na_{i/e}$ , and  $Cl_{i/e}$ .

For  $I_{app} = 0$  this model is monostable with an equilibrium at  $V = -68$  mV. Note that  $E_{Na} \neq V$  and  $E_K \neq V$  imply that under equilibrium conditions neither  $I_{Na^+}$  nor  $I_{K^+}$  vanish, but only their sum does. Sufficiently strong current pulses can—depending on their duration—initiate single voltage spikes or spike trains. Constant applied currents can drive the system to a regime of stationary oscillations. The minimal current required for this is usually called rheobase current.

The HH model can be reduced to two dynamical variables in a way that preserves these dynamical features. One common simplification [35] is to eliminate the fastest gating variable  $m$  adiabatically and set

$$m = m_{\infty}(V). \quad (15)$$

Second, there is an approximate functional relation between  $h$  and  $n$  that is usually realized as a linear fit [36]. The ion-based model presented in this article, however, contains a stable fixed point with large  $n$ , and a linear best fit would then lead to a negative  $h$ . Therefore we will use the following sigmoidal fit to make sure  $h$  is non-negative:

$$h = h_{sig}(n) = 1 - \frac{1}{1 + \exp(-6.5(n - 0.35))}. \quad (16)$$

After this reduction the remaining dynamical variables are  $V$  and  $n$ .

### Minimal ion-based model

While in the original HH model ion concentrations are model parameters, in ion-based modeling intra- and extracellular ion

concentrations become dynamical variables, which causes the Nernst potentials to be dynamic. The model defined by the rate eqs. (1), (2) and constraint eqs. (15), (16) can straightforwardly be extended to make ion concentrations dynamic since currents induce ion fluxes. However, under those equilibrium conditions found in HH neither  $I_{K^+} = 0$  nor  $I_{Na^+} = 0$ . Hence we need to include ion pumps [15] to make sure that the rate of change in ion concentration inside the cell ( $i$ ) and extracellular ( $e$ ) can vanish in the resting state ( $\dot{N}a_{i/e} = \dot{K}_{i/e} = \dot{C}l_{i/e} = 0$ ).

The rate equations for ion concentrations in the intracellular space (ICS) are then

$$\frac{dNa_i}{dt} = -\frac{\gamma}{\omega_i}(I_{Na^+} + 3I_p), \quad (17)$$

$$\frac{dK_i}{dt} = -\frac{\gamma}{\omega_i}(I_{K^+} - 2I_p), \quad (18)$$

$$\frac{dCl_i}{dt} = +\frac{\gamma}{\omega_i}I_{Cl^-}. \quad (19)$$

The factor  $\gamma$  converts currents to ion fluxes and depends on the membrane surface  $A_m$  and Faraday's constant  $F$ :

$$\gamma = \frac{A_m}{F}, \quad (20)$$

Dividing the ion fluxes by the ICS volume  $\omega_i$  gives the change rates for the ICS ion concentrations. The pump current  $I_p$  represents the ATP-driven exchange of ICS sodium with potassium from the extracellular space (ECS) at a 3/2-ratio. It increases with the ICS sodium and the ECS potassium concentration. Chloride is not pumped. We are using the pump model from [23,24]:

$$I_p(Na_i, K_e) = \rho \left(1 + \exp\left(\frac{25 - Na_i}{3}\right)\right)^{-1} \left(1 + \exp(5.5 - K_e)\right)^{-1}, \quad (21)$$

where  $\rho$  is the maximum pump current. As a consequence of mass conservation ion concentrations in the ECS can be computed from those in the ICS [33]:

$$ion_e = ion_e^{(0)} + \frac{\omega_i}{\omega_e}(ion_i^{(0)} - ion_i), \quad (22)$$

with the ECS volume  $\omega_e$ . Superscript zero indicates initial values. Since all types of transmembrane currents, i.e., also the pumps, must be included in eq. (1) for the membrane potential, we have to add the net pump current  $I_p$ :

$$\frac{dV}{dt} = -\frac{1}{C_m}(I_{Na^+} + I_{K^+} + I_{Cl^-} + I_p - I_{app}). \quad (23)$$

The rate equations for the ion-based model are thus given by eqs. (2), (17)–(19), (23). These rate equations are complemented by the gating constraints eqs. (15), (16) and the mass conservation constraints

$$Na_e = Na_e^{(0)} + \frac{\omega_i}{\omega_e}(Na_i^{(0)} - Na_i), \quad (24)$$

$$K_e = K_e^{(0)} + \frac{\omega_i}{\omega_e}(K_i^{(0)} - K_i), \quad (25)$$

$$Cl_e = Cl_e^{(0)} + \frac{\omega_i}{\omega_e}(Cl_i^{(0)} - Cl_i). \quad (26)$$

Dynamic ion concentration imply that the Nernst potentials in eqs. (11)–(13) are now dynamic (see eq. (14)). The additional parameters of the ion-based model are listed in Table 2. The morphological parameters  $A_m$  and  $\omega_i$  are taken from [17]. In cortical ion-based models, the extracellular volume fraction  $f = \omega_e/(\omega_e + \omega_i)$  ranges from 13% in [17] to 33% in [21]. In experimental studies,  $f$  is about 20%, a value that can increase, for example, in focal cortical dysplasias type II, a frequent cause of intractable epilepsy, to 27% [37] or during sleep to 32% (the latter only, if we transfer the increase observed in mouse data to human) [38]. It is important to note that in experimental studies, the extracellular volume fraction refers to the fraction with respect to the whole tissue, which includes also the glial syncytium. Assuming equally sized neuronal and glial volume fractions of 40% each, an experimentally measured value of 20% would in our model, which does not directly include the volume of the glial syncytium, correspond to  $f = 0.33$  or 33%. We choose an intermediate value of 25% for  $f$ , but address the influence of the volume ratio in Sec. Results. We prefer to give these morphological parameters in the commonly used units which are appropriate to their order of magnitude rather than unifying all parameters, e.g. the cell volume is given in  $\mu\text{m}^3$  instead of  $l$  which ion concentrations are related to. Consequently  $\gamma$  from Table 2 must be multiplied by a factor of 10 to correctly convert currents to change rates for ion concentration in the given units. Because of the extremely small value of  $\gamma$  the membrane dynamics, i.e., the dynamics of  $V$  and  $n$ , is five orders of magnitude faster than the ion dynamics.

A consequence of this large timescale separation is that the system will attain a Donnan equilibrium when the pumps break down. The Donnan equilibrium is a thermodynamic equilibrium state (not to be confused with merely a fixed point, though it is one) that is reached for ion exchange across a semipermeable membrane. Since we have not explicitly included large impermeable anions inside the cell, this is at first surprising. For no applied currents and  $I_p = 0$ , the ion rate equations imply that an equilibrium requires all ion currents to vanish. Since conductances

**Table 2.** Model parameters for ion-based model only.

Name	Value & unit	Description
$\omega_i$	2,160 $\mu\text{m}^3$	volume of ICS
$\omega_e$	720 $\mu\text{m}^3$	volume of ECS
$F$	96485 C/Mol	Faraday's constant
$A_m$	922 $\mu\text{m}^2$	membrane surface
$\gamma$	9.556e-3 $\frac{\mu\text{m}^2\text{Mol}}{\text{C}}$	conversion factor
$\rho$	5.25 $\mu\text{A}/\text{cm}^2$	max. pump current

doi:10.1371/journal.pcbi.1003551.t002

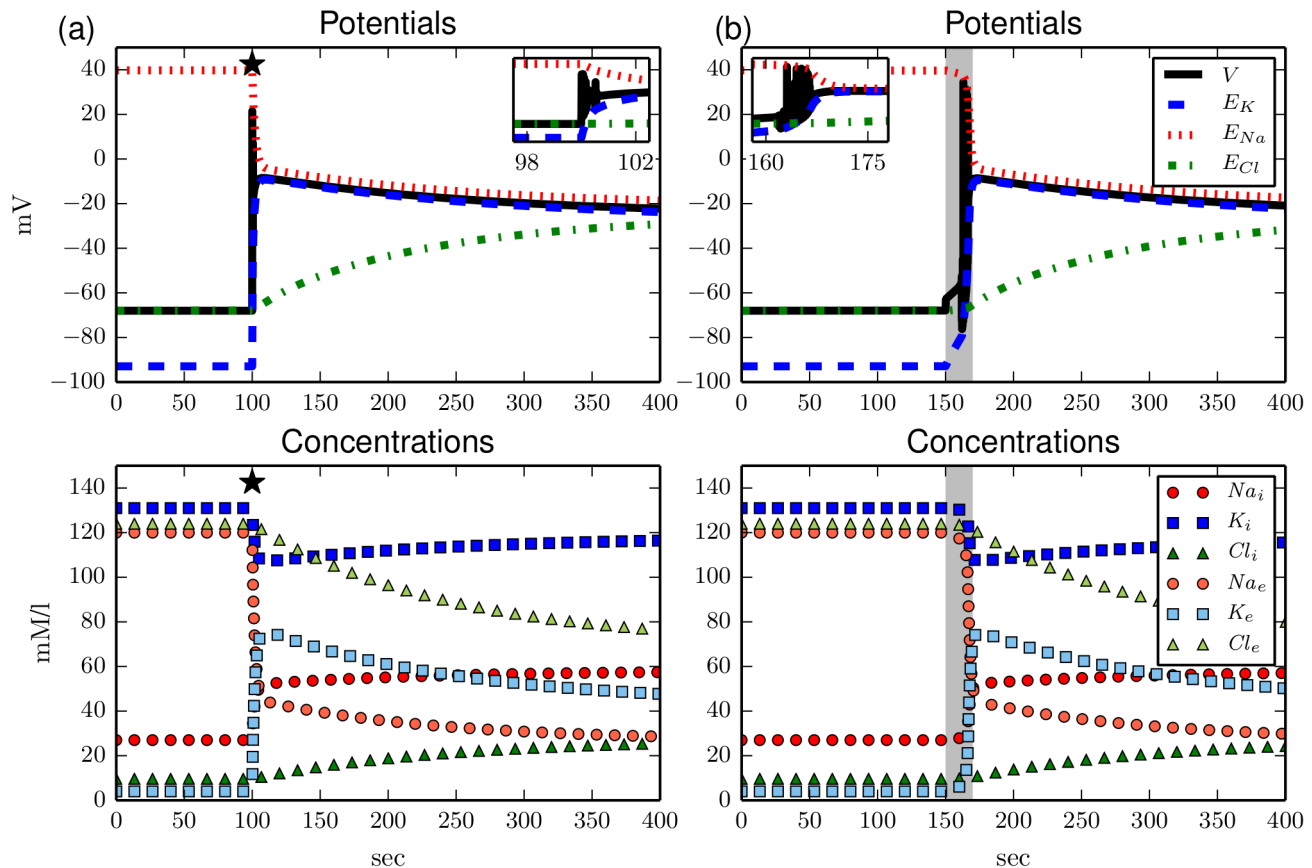


**Figure 1. Upper panels: Membrane and Nernst potentials, lower panel: Ion concentrations vs time.** (a) Response of the model to a 0.5 sec long sodium current pulse with amplitude  $150 \mu\text{A}/\text{cm}^2$  (marked by the black star). The pulse causes voltage spiking that stops in a strongly depolarized state (see blow-up inset). The membrane potential  $V$  takes a final value of about  $-25 \text{ mV}$  (upper panel). The ion gradients, i.e., the differences between intra- and extracellular ion concentrations, reduce drastically during the stimulation and slowly adjust to a new fixed point after a couple of hundreds of seconds (lower panel). (b) Switching off the ion pump for 20 sec (indicated by the light grey interval) causes similar dynamics. The membrane depolarization and dissipation of ion gradients is a bit slower than for (a). After the pump is switched on again the system attains the same fixed point as in (a).  
 doi:10.1371/journal.pcbi.1003551.g001

are strictly positive it follows that all Nernst potentials and the membrane potential must be equal. Ion concentrations will then adjust accordingly. However, eqs. (17)–(19) and (23) imply the following constraint on the ICS charge concentration  $Q_i$ :

$$\Delta Q_i := \Delta Na_i + \Delta K_i - \Delta Cl_i = \frac{C_m \gamma}{\omega_i} \Delta V, \quad (27)$$

where  $\Delta$  denotes the difference between the initial and final value of a variable. Since  $\gamma$  is very small, changes in ion concentrations must practically satisfy electroneutrality. This condition together with the equality of all Nernst potentials defines the Donnan equilibrium, so we see that it is contained in our model as the limit case with no pumps and no applied currents. It should be noted that this observation provides a necessary condition for the correctness of biophysical models.

In this extension of the HH model the ion dynamics makes Nernst potentials time-dependent. The simultaneous effect of a diffusive and an electrical force acting on a solution of ions is described more accurately by the Goldman–Hodgkin–Katz (GHK) equation though. Nevertheless we prefer Nernst currents, because this formulation allows us to use well-established conductance parameters so that the model is

completely defined by empirically estimated parameters. In Sec. Results we will see how GHK currents can be modelled and that the qualitative dynamical behaviour of the system is not affected.

## Results

### Phase space analysis of ion-based model

In the ion-based model introduced above current pulses can still initiate voltage spikes (not shown). However, extremely strong pulses, in fact comparable to those used in [17] to trigger spreading depolarizations, can drive the system away from the physiological equilibrium to a second stable fixed point that is strongly depolarized (see Fig. 1(a)). This is a new dynamical feature. The depolarized state can also be reached when the ion pumps are temporarily switched off (see Fig. 1(b)). Apart from the depolarization this state is characterized by almost vanishing ion gradients. This free energy-starvation (FES) is reminiscent of the Donnan equilibrium. Extracellular potassium is increased from 4 to more than 40 mMol/l while the extracellular sodium concentration is reduced from 120 to less than 30 mMol/l. The gated ion channels are mostly open (potassium activation  $n$  is 60%), and it is no longer possible to initiate voltage spikes. In this section we will



present a phase space analysis of the model and derive conditions for the observed bistability between a physiological equilibrium and a state of FES.

Note that the transition from the physiological state to FES happens via ion accumulation due to spiking, and we will see in Sec. Results that indeed the membrane ability to spike is a necessary condition for the bistability. Similar processes of ion accumulation were regarded as unphysiological in modelling of cardiac cells [8], but are familiar in cortical neurons where ion accumulation is central to seizure-like activity [24,33] and spreading depression [17] (SD). In fact, we will briefly demonstrate how the bistability relates to local SD dynamics.

**Symmetry of the ion-based model.** Prior to a bifurcation analysis we need to discuss a conservation law (symmetry) of eqs. (17)–(19), (23). The direct extension of a membrane model to include ion dynamics as presented above naturally leads to a linear dependence of dynamical variables. In our case this is reflected by the following relation

$$C_m \frac{dV}{dt} = \frac{\omega_i}{\gamma} \left( \frac{dNa_i}{dt} + \frac{dK_i}{dt} - \frac{dCl_i}{dt} \right), \quad (28)$$

for  $I_{app}=0$ . As a consequence the determinant of the Jacobian is always zero and the system is nowhere hyperbolic. For the continuation techniques used by software tools like AUTO [39], however, the inverse Jacobian plays a central role, so they cannot be applied to the system unless this degeneracy is resolved. Furthermore the phase space structure of such nonhyperbolic systems can be changed with arbitrarily small perturbations which is why they are called structurally unstable [40]. Note that the linear dependence can be avoided when the rate equation for  $V$  contains an additional current with a fixed reversal potential breaking the symmetry. Such strictly speaking unphysical currents are indeed often included in neuronal ion-based models [17,24,33,34], but we will rather make use of the symmetry and eliminate one linearly dependent variable.

The physiological view on the instability should be as follows. Assume that the system is in its physiological equilibrium and then apply a constant current  $I_{app}$  to the voltage rate eq. (23). Then eqs. (17)–(19) and (23) imply that the equilibrium conditions  $\dot{V}=0$  and  $\dot{K}_i = \dot{Na}_i = \dot{Cl}_i = 0$  are contradictory, so the equilibrium will vanish even for arbitrarily small currents. In fact for any constant and positive  $I_{app}$ , the system will evolve in a highly non-physiological manner with  $K_i$ ,  $Na_i$  and  $Cl_e$  slowly tending to zero.

To avoid even the theoretical possibility of such behaviour we will now use eq. (28) to reduce the system and thereby make it structurally stable. We can, for example, eliminate  $V$  and express it in terms of the ICS ion concentrations rather than treating  $V$  as an independent dynamical variable:

$$\frac{d}{dt} \left( V - \frac{\omega_i}{C_m \gamma} (Na_i + K_i - Cl_i) \right) = 0$$

⇒

$$V = V^{(0)} + \frac{\omega_i}{C_m \gamma} \left( Na_i - Na_i^{(0)} + K_i - K_i^{(0)} - Cl_i + Cl_i^{(0)} \right)$$

This was also done in Ref. [15]. The physiological meaning of this reduction is simply that the possibility of unspecified applied currents is ruled out. For instance, a perturbation on the sodium

rate eq. (17) should be interpreted as a sodium current. The above constraint describes the simultaneous effect on  $V$ . It would be equivalent to apply perturbations to eq. (17) and eq. (23) consistently to model the full effect of an applied sodium current, so the additional constraint should be seen as a consistency condition. (The curves in Fig. 1(a) were computed for a sodium current pulse.) This consistency rule does not at all change the dynamics unless unspecified currents are applied, and even then it practically does not change the dynamics, because any deviation in ion concentrations scales with  $\gamma$  and is hence negligible. The structural instability is thus a rather formal feature of the degenerate model and we remark that its physiological equilibrium is nevertheless stationary. Instabilities that lead to an unphysiological drift of ion concentrations for very long simulation times have been reported and resolved in cardiac cell models [7,8]. Our case is different though, because the physiological state is a stationary one and the response to moderate stimulation is physiologically realistic.

For the bifurcation analyses presented in this paper we have eliminated  $Na_i$  rather than  $V$  for numerical reasons. This is completely equivalent, because we only vary the pump rate and morphological parameters. So in our reduction we have replaced rate eq. (17) by the following constraint:

$$Na_i = Na_i^{(0)} - K_i + K_i^{(0)} + Cl_i - Cl_i^{(0)} + \frac{C_m \gamma}{\omega_i} (V - V^{(0)}) \quad (29)$$

The model is then defined by the rate eqs. (2), (18), (19) and (23) and the constraint eqs. (15), (16), (24)–(26) and (29).

**Bifurcation analysis.** We have used the continuation tool AUTO [39] to follow the polarized fixed point of the system under variation of the maximal pump rate  $\rho$ . Stability changes and the creation of stable or unstable limit cycles are detected by the software which helps us to interpret the dynamical behaviour. For a better overview we will extend our bifurcation analysis even beyond the physiologically relevant range. The full bifurcation diagram is presented in Fig. 2.

In the  $(\rho, V)$ -plane the fixed point continuation yields a smooth z-shaped curve where unstable sections are dashed. The physiological equilibrium is marked by a green square. For higher pump rates the equilibrium remains stable and becomes slightly hyperpolarized. If  $\rho$  is decreased the physiological equilibrium collides with a saddle point at  $\rho_{LP1} = 0.894006 \mu\text{A}/\text{cm}^2$  in a saddle-node bifurcation (limit point, LP). In a LP the stability of a fixed point changes in one direction (zero-eigenvalue bifurcation). Thus after LP1 the fixed point is a saddle point with one unstable direction. In a Hopf bifurcation (HB) at  $\rho_{HB1} = 29.2336 \mu\text{A}/\text{cm}^2$  two more directions become unstable. Via another LP at  $\rho_{LP2} = 34.5299 \mu\text{A}/\text{cm}^2$  the last stable direction switches to unstable and the saddle becomes an unstable node. In HBs at  $\rho_{HB2} = 33.7285 \mu\text{A}/\text{cm}^2$  and  $\rho_{HB3} = 24.6269 \mu\text{A}/\text{cm}^2$  the fixed point becomes a saddle and a stable depolarized focus, respectively. The stability is indicated by the  $(n_-, n_+)$ -tuples along the fixed point curve with  $n_{-,+}$  denoting the number of stable and unstable directions.

In every HB a limit cycle is created. Our model only contains unstable limit cycles that are created in subcritical HBs. In the diagram they are represented by their extremal  $V$  values. Such unstable limit cycles are not directly observable, but in the bistable regime they can play a role for the threshold behaviour for the transition from one fixed point to the other. All limit cycles in the model disappear in homoclinic bifurcations (HOM). In a HOM a

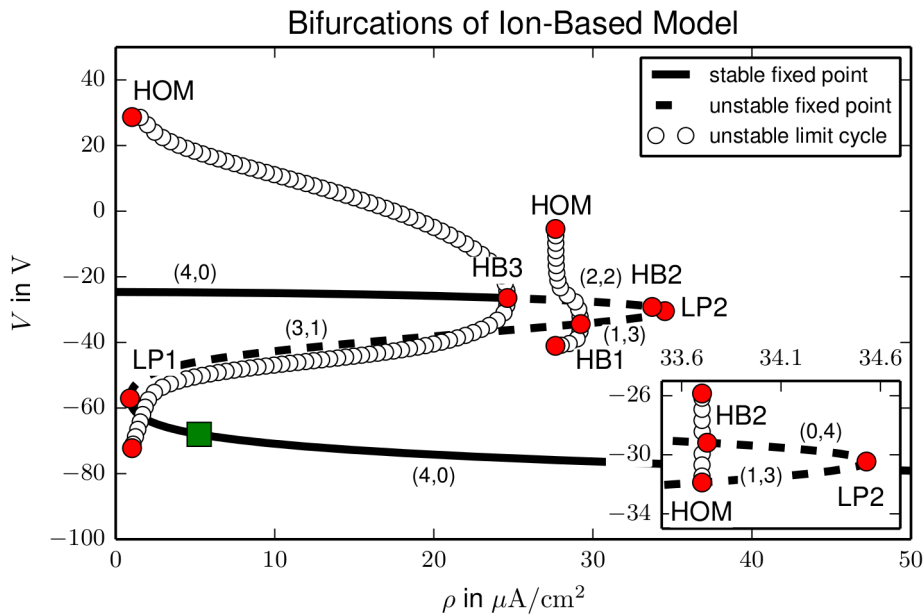


**Figure 2. Bifurcation diagram of the ion-based model.** Bifurcations are marked by red circles, the physiological equilibrium by a green square. Following the z-shaped fixed point characteristic from below there are two saddle-node bifurcations (limit point, LP) at  $\rho = 0.894006 \mu\text{A}/\text{cm}^2$  and  $\rho = 34.5299 \mu\text{A}/\text{cm}^2$ , and three subcritical Hopf bifurcations (HB) at  $\rho = 29.2336 \mu\text{A}/\text{cm}^2$ ,  $\rho = 33.7285 \mu\text{A}/\text{cm}^2$  and  $\rho = 24.6269 \mu\text{A}/\text{cm}^2$ . The limit cycles created in HB1, HB2 and HB3 disappear in homoclinic bifurcations (HOM) at  $\rho = 27.6463 \mu\text{A}/\text{cm}^2$ ,  $\rho = 33.7027 \mu\text{A}/\text{cm}^2$  and  $\rho = 1.024291 \mu\text{A}/\text{cm}^2$ , respectively. The second LP and the second HB together with the HOM of limit cycles occur in a very narrow parameter range (see blow-up inset). The number of stable ( $n_-$ ) and unstable ( $n_+$ ) directions of the fixed point is indicated by the  $(n_-, n_+)$ -tuples. There is bistability of a physiological state and a depolarized state with largely reduced ion concentration gradients between  $\rho = 8.94006 \mu\text{A}/\text{cm}^2$  and  $\rho = 24.6269 \mu\text{A}/\text{cm}^2$ . doi:10.1371/journal.pcbi.1003551.g002

limit cycle collides with a saddle. When it touches the saddle it becomes a homoclinic cycle of infinite period. After the bifurcation the limit cycle does not exist any more. The limit cycles created in HB1, HB2 and HB3 disappear in HOMs at  $\rho = 27.6463 \mu\text{A}/\text{cm}^2$ ,  $\rho = 33.7027 \mu\text{A}/\text{cm}^2$  and  $\rho = 1.024291 \mu\text{A}/\text{cm}^2$ . The limit cycle emanating from HB1 collides with the upper (i.e., less polarized) saddle, for the other two HOMs the situation is clear, because there is only one saddle available. Since the limit cycles are all unstable these bifurcation details are physiologically irrelevant, but mentioned for completeness.

This bifurcation analysis shows that our model is bistable for a large range of pump rates  $\rho_{LP1} < \rho < \rho_{HB3}$ . Strongly depolarized and electrically inactive states of neurons with nearly vanishing ion concentration gradients have been reported in pathological states [11,13], but in real systems such free energy-starvation (FES) is not stable. In the below section we show how this bistability can be resolved.

**Ionic excitability.** We will now briefly show how the above analyzed model can be modified such that the unphysiological bistability turns into excitability of ion dynamics. For this we follow [24,33] and include an additional regulation term for extracellular potassium. This means that  $K_e$  becomes an independent dynamical variable and the constraint eq. (25) must be replaced by its rate equation:

$$\frac{dK_e}{dt} = \frac{\gamma}{\omega_e} (I_{K^+} - 2I_p) + I_{reg}. \quad (30)$$

The regulation term  $I_{reg}$  can be interpreted as a diffusive coupling to an extracellular potassium bath or as a phenomenological buffering term. It takes the following form:

$$I_{reg} = \lambda(K_{reg} - K_e), \quad (31)$$

where  $K_{reg}$  is the potassium concentration of an infinite bath reservoir coupled to the neuron or a characteristic parameter for glial buffering, and  $\lambda$  is a rate constant (values given in Table 3).  $K_{reg}$  takes values of physiological potassium concentrations and hence stabilizes the physiological equilibrium. This is how  $I_{reg}$  regulates ion homeostasis and destabilizes the energy-starved state.

If we now stimulate the system with a current pulse or temporarily switch off the pump as we did in Fig. 1 the system no longer remains in the depolarized state, but repolarizes after a long transient state of FES (see Fig. 3). After the repolarization ion concentrations start to recover from FES. Full recovery to the initial physiological values is an asymptotic process which takes very long (about two hours), but the neuron is back to normal functioning already after nine to ten minutes. Similar dynamics is described in numerical [17,34] and experimental SD models.

The bistable and excitable dynamics can be nicely compared in a projection of the respective trajectories onto the  $(Na_i, K_i)$ -plane.

**Table 3. Buffering parameters.**

Name	Value & unit	Description
$\lambda$	2.7e-5/msec	regulation rate
$K_{reg}$	4 mMol/l	regulation level

doi:10.1371/journal.pcbi.1003551.t003

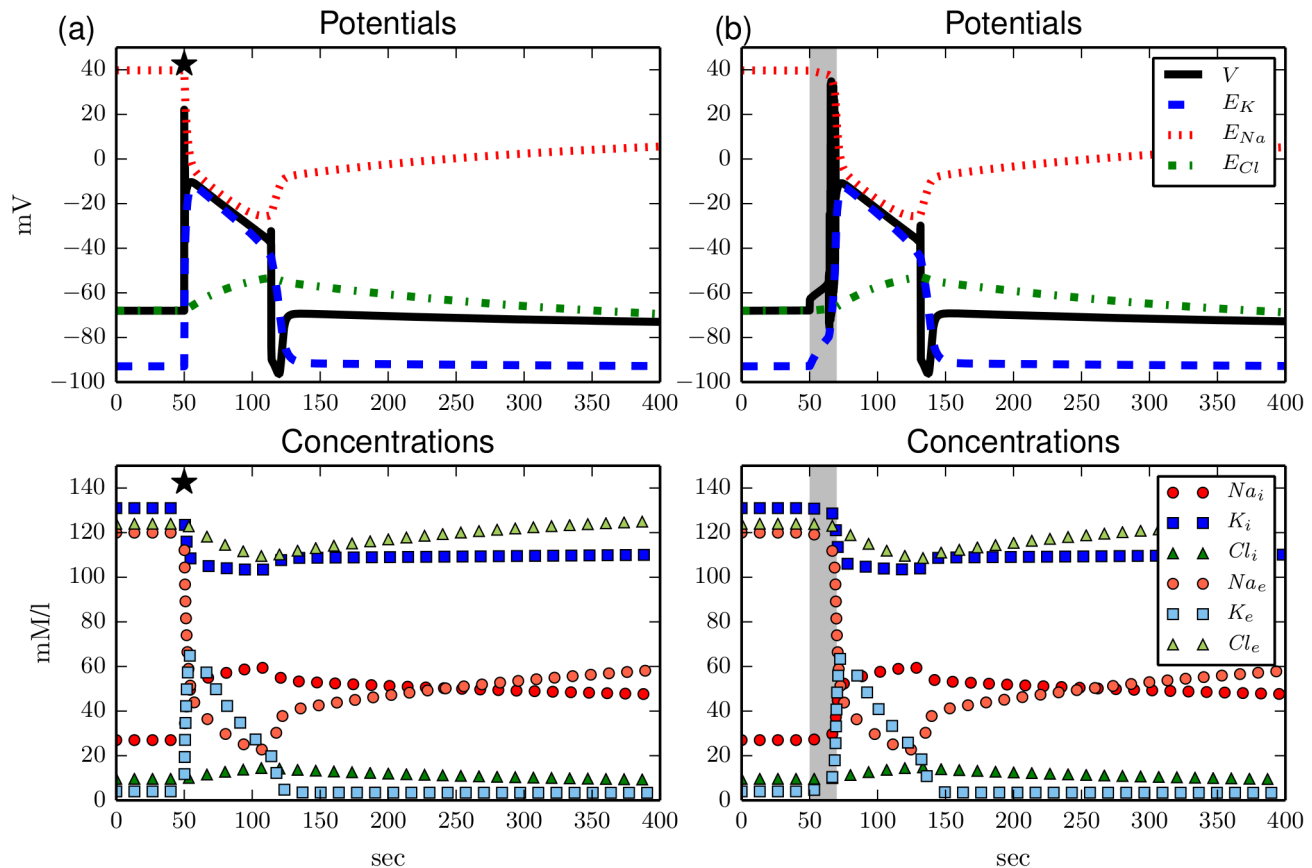


**Figure 3. Upper panels: Membrane and Nernst potentials, lower panel: Ion concentrations vs time.** (a) Stimulation with the same, but earlier applied, current pulse as in Fig. 1(a). Due to the additional potassium regulation the system returns to the physiological equilibrium after an approximately 60 sec lasting FES and subsequent hyperpolarization. (b) Similar dynamics as in (a) is observed for a temporary pump switch-off like in Fig. 1(b). doi:10.1371/journal.pcbi.1003551.g003

For the bistable model the conditions  $\dot{K}_i = 0$  and  $\dot{Na}_i = 0$  define three-dimensional hypersurfaces called nullclines. Adding the necessary fixed point conditions on the remaining dynamical variables, namely  $V = E_{Cl}$  and  $n = n_\infty(V)$ , allows us to specify curves that represent these nullclines and only depend on  $Na_i$  and  $K_i$ . In the buffered model  $K_e$  is another dynamical variable and its fixed point condition is  $K_e = K_{reg}$ . Electroneutrality and mass conservation imply that certain  $(Na_i, K_i)$ -combinations would lead to a negative  $Cl_i$  or  $K_e$ . In the plot, these unphysiological configurations are shaded.

In Fig. 4, we see that the bistable model has three nullcline intersections, i.e., fixed points, while the buffering term deforms the nullclines so that only one stable fixed point remains. In the bistable case an initial current pulse stimulation (dashed part of trajectory) drives the system into the basin of attraction of the FES-state, which it then asymptotically approaches (solid line). After the same stimulation the buffered system performs a large excursion in phase space with extremal ion concentrations comparable to FES, but eventually returns to the physiological equilibrium. This large excursion in the ionic variables characterizes what we refer to as ionic excitability or excitability of ion homeostasis. The simulations presented in this section support the hypothesis that it is caused by the bistability of the unbuffered model. Note that intersections of nullcline curves and trajectories do not have to be horizontal or vertical since they may (and do) differ in the non-ionic variables. The main purpose of the nullcline curves is to indicate the existence and location of fixed points.

### Robustness of results

The ion-based model we have analysed so far has been motivated as a natural extension of the Hodgkin-Huxley membrane model. However, there are different variants of ion-based models [17–24,32] that use different pump and current models, ion content, and ion channels. We will hence address the question how general our results are in this respect. Furthermore we vary the geometry-dependent parameters (membrane surface and extracellular volume fraction) continuously to test their effect on the phase space, too.

**Model variants.** As we noted before, transmembrane currents are more accurately described as Goldman-Hodgkin-Katz (GHK) rather than Nernst currents, even though we prefer the latter. It is hence important to check which difference the choice of current model makes. To generalize the Nernst currents in eqs. (11)–(13) to GHK currents we assume that both models have the same steady state currents under physiological equilibrium conditions. The GHK version of the sodium current is

$$I_{Na^+}^{GHK} = (P_{Na}^l + P_{Na}^g m^3 h) \cdot F \cdot \frac{V}{26.64} \cdot \frac{Na_i - Na_e \exp(-V/26.64)}{1 - \exp(-V/26.64)} \quad (32)$$

with membrane permeabilities  $P_{Na}^l$  and  $P_{Na}^g$  instead of conductances. To compute these permeabilities we set the GHK current



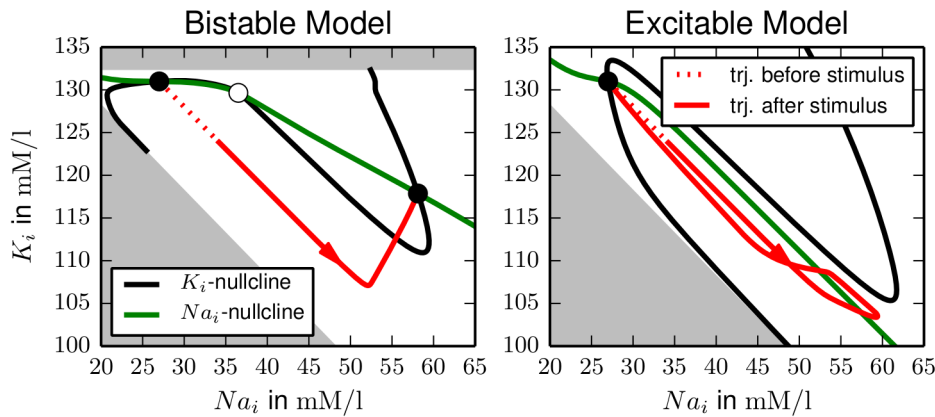


**Figure 4. Projection of the trajectories corresponding to Fig. 1a and Fig. 3a.** The shaded regions indicate unphysiological ( $Na_i, K_i$ )–combinations that imply negative  $Cl_i$  (lower left region) or negative  $K_e$  (upper region in left plot). Stable and unstable fixed points are marked by solid and open circles. (a) In the bistable case an initial stimulation (dashed line) leads to large subsequent changes in ion concentrations that terminate in the second fixed point of the system. (b) The excitable motion starts very similar to case (a), but after reaching the extremal concentration values the system slowly returns to its initial state.  
doi:10.1371/journal.pcbi.1003551.g004

equal to its Nernstian counterpart

$$I_{Na^+} = (g_{Na}^l + g_{Na}^g m^3 h) (V - E_{Na}) \quad (33)$$

for the equilibrium conditions given in Table 1. This leads to a common conversion factor from conductances  $g_{Na}^{l,g}$  to permeabilities  $P_{Na}^{l,g}$ . With this ansatz we obtain conversion factors for the three different ion species that lead to the conductances listed in Table 4.

There is also a certain freedom in the choice of a pump model. It is a general feature of  $Na^+/K^+$  pumps that their activity is enhanced by the elevation of ECS potassium and ICS sodium. Still different models exist, and to investigate the role of the particular pump model we replace the pump from eq. (21), now referred to as  $I_{p,A}$ , with the following one from [17]:

$$I_{p,B}(Na_i, K_e) = \rho_B \left(1 + \frac{3.5}{K_e}\right)^{-2} \left(1 + \frac{10}{Na_i}\right)^{-3} \quad (34)$$

In order to retain the equilibrium at  $V = -68$  mV we have to set the maximum pump current to  $\rho_B = 5.72 \mu A/cm^2$ . This is slightly higher than the previous pump value ( $\rho_A = 5.25 \mu A/cm^2$ ), but in the same range.

From the rate equations of the HH membrane model (see Sec. Model) it is obvious that the chloride leak current stabilizes the equilibrium membrane potential. To test its stabilizing effect in the

**Table 4. Membrane permeabilities for GHK current.**

Name	Value & unit	Description
$P_{Na}^l$	0.0264 $\mu m/sec$	leak sodium permeability
$P_{Na}^g$	150.77 $\mu m/sec$	gated sodium permeability
$P_{K}^l$	0.0169 $\mu m/sec$	leak potassium permeability
$P_{K}^g$	13.488 $\mu m/sec$	gated potassium permeability
$P_{Cl}^l$	0.0521 $\mu m/sec$	leak chloride permeability

doi:10.1371/journal.pcbi.1003551.t004

context of ion-based modeling we compare models that either do or do not contain this current. We are further interested in the question whether membrane excitability and ion bistability are related. Therefore also the effect of in- and excluding active ion channels is tested.

In this section we will only discuss fixed points and their stability, but not the unstable limit cycles belonging to HBs. In Fig. 5 the fixed point continuation curves for all combinations of current model (Nernst or GHK), pump choice ( $I_{p,A}$  or  $I_{p,B}$ ) and the respective in- and exclusion of chloride and active ion channels are shown. Each panel (a)–(d) contains all continuation curves for a given choice of pump and current model. For those models that are bistable for certain pump rates an overview of the different dynamical regimes is presented in Fig. 6. It shows the parameter ranges for bistability and for monostability of a physiological state or FES.

The most striking result of this bifurcation analysis is that this bistability occurs in all models with gated ion channels, but not in any model with only leak channels (grey-shaded graphs in the insets of Fig. 5). The comparison of any model with active gates and its leak-only counterpart shows that whenever the physiological equilibrium of the first one exists it is identical to the equilibrium of the latter one. While the physiological state disappears in a LP for all bistable models at small pumping, the fixed points of the leak models remain stable, but depolarize drastically for further decreasing pump rates until the Donnan equilibrium for  $\rho_{A,B} = 0$  is reached. The absence of the second fixed point in leak-only models is plausible if we consider Fig. 1 again. The depolarized state is characterized by large ion concentrations  $K_e$  and  $Na_i$  which implies an increased pump current (see eq. (21)). Since the differences between the Nernst potentials and the membrane potential are even smaller in the depolarized state, higher, hence gated, conductances are required to compensate for the pump currents and maintain the depolarized state. Besides the requirement of active ion channels, the bistability is a very robust feature of these simple ion-based models.

Let us now consider the effect of the different model features on the minimal physiological pump rate, i.e., the pump rate required for a stable physiological fixed point, and the recovery pump rate that destabilizes the depolarized state of FES and allows the

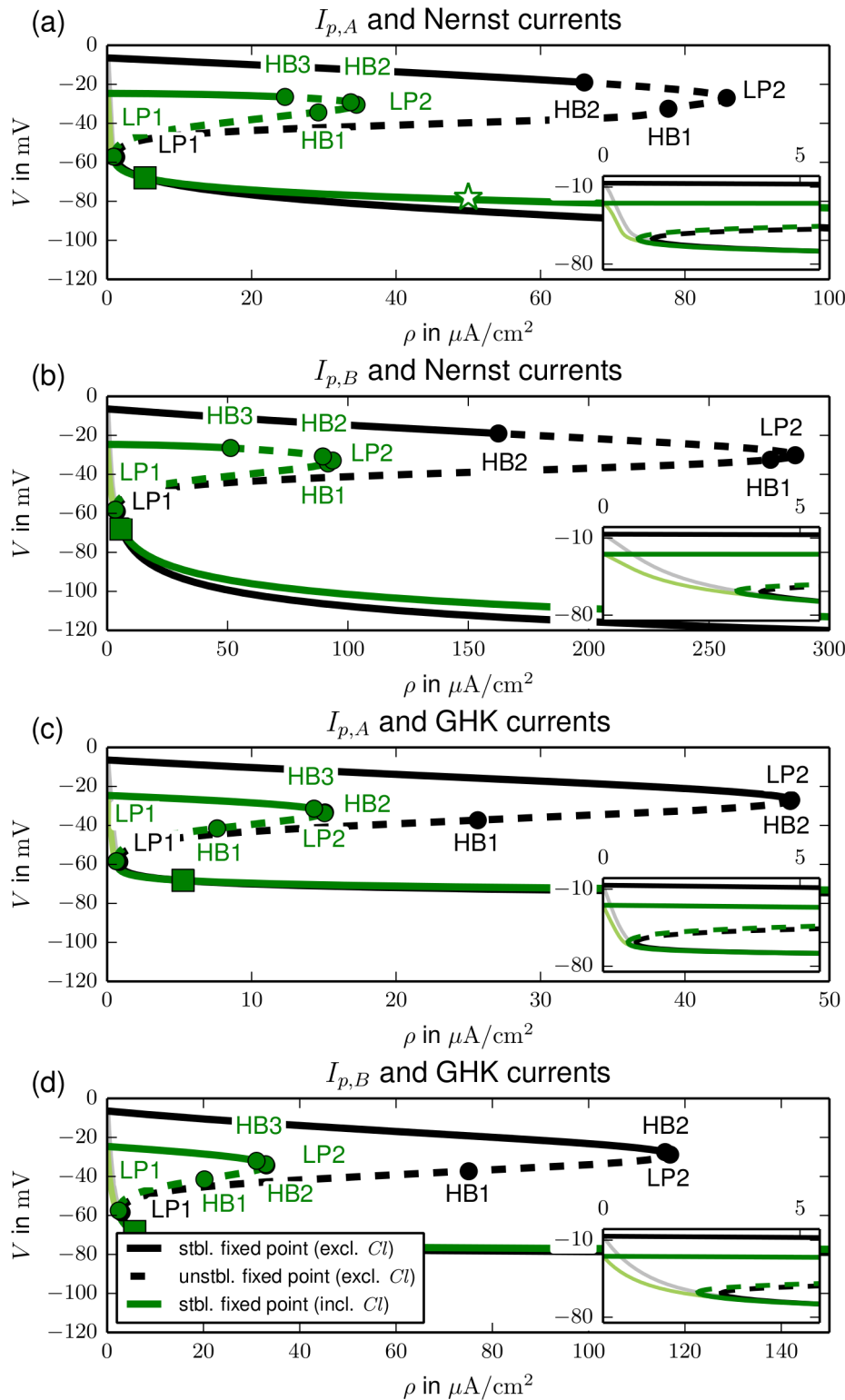


**Figure 5. Bifurcation diagrams of fixed points for different models.** The effects of chloride and active ion channels are compared for each of the four possible pump (A vs B) and current model (Nernst vs GHK) combinations. The physiological equilibrium for normal pump rates ( $\rho_A = 5.25 \mu\text{A}/\text{cm}^2$  and  $\rho_B = 5.72 \mu\text{A}/\text{cm}^2$ ) is marked by a green square. The model from fig. 2 is marked by a star. The value is the same with and without chloride or active channels. Insets show the bifurcation diagrams for low pump rates ( $\rho_{A,B} < 5 \mu\text{A}/\text{cm}^2$ ). Fixed point lines for models without active ion channels are shaded (see insets). Note the different scales on the main figures, insets are for the same range in each panel. doi:10.1371/journal.pcbi.1003551.g005

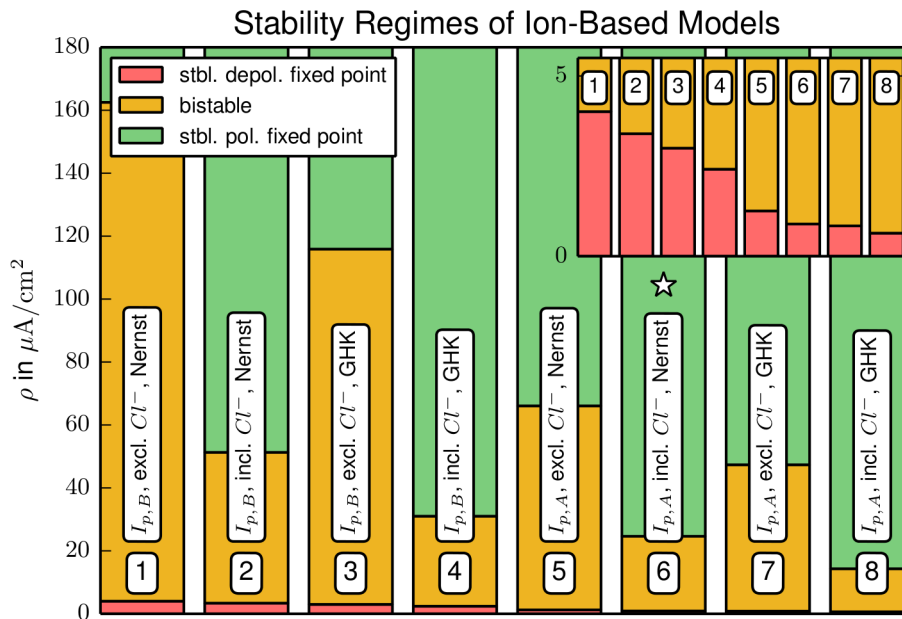


**Figure 6. Overview of the parameter regimes for bistability, polarized and depolarized stability for different models (1–8).** The change from the monostable depolarized regime to bistability (red to orange) defines the minimal physiological pump rate, i.e., the pump rate required for the existence of a polarized fixed point. The line separating the bistable from the monostable polarized regime (orange to green) defines the minimal recovery pump rate, i.e., the pump rate required to return from the depolarized fixed point to the polarized equilibrium. The model from Sec. Model is marked by a star. doi:10.1371/journal.pcbi.1003551.g006

neuron to return to physiological conditions. These rates are the lower and upper limit of the bistable regime, and low values are physiologically desirable.

In Fig. 6 we see that pump model A, GHK currents and chloride each lead to a lower minimal physiological (see the inset) and a lower recovery pump rate than pump model B, Nernst currents and the exclusion of chloride. Quantitative differences should be noted, though. The inset of Fig. 6 shows that all models with pump A have lower minimal physiological pump rates than models with pump B. So the stability of the physiological equilibrium with respect to pump strength reduction depends mostly on the choice of pump. On the other hand four of the five lowest recovery pump rates are from models that include chloride. In fact, it is only the combination of both, the GHK current model and pump A, that make the recovery threshold of the chloride excluding model 7 slightly lower than that of the chloride including model 2. However, one should note that even the lowest recovery pump rate is as high as  $\rho = 14.3 \mu\text{A}/\text{cm}^2$  (model 8). This is still an almost threefold increase of the normal rate. So even if we assume pump enhancement due to additional mechanisms, for example increased cerebral blood flow, the threshold for recovery from FES seems to be too high. Thus it is true for a large class of ion-based neuron models that realistic neuronal homeostasis cannot rely on  $\text{Na}^+/\text{K}^+$ -ATPase alone, but rather on a combination of ion pumps and further regulation mechanisms like glial buffering.

There is another effect of chloride to be pointed out. In Fig. 5 we see that it raises the Donnan equilibrium potential (see potentials at  $\rho = 0 \mu\text{A}/\text{cm}^2$ ) significantly. To understand this effect note that without chloride electroneutrality forces the sum of  $\Delta K_e$  and  $\Delta Na_e$  to be zero, while the presence of the decreasing anion species  $Cl_e$  implies  $\Delta(K_e + Na_e) < 0$ . According to eq. (14) this leads to lower Donnan equilibrium Nernst potentials  $E_K$  and  $E_{Na}$ ,

and consequently to a lower membrane potential. Since the conditions of FES for physiological pump rate values are very close to the Donnan equilibrium, this depolarized fixed point is shifted in the same way.

The effect of the current model on the two characteristic pump rates is less pronounced than that of chloride or the pump choice. It lowers the minimal physiological rate more than chloride, but not as much as a pump change from model B to A. Its effect on the recovery threshold is the weakest.

While above we describe and investigate minimal Hodgkin–Huxley model variants to obtain SD behavior in the simplest neuron model types, in the current literature biophysically much more detailed neuron models have been developed for this phenomenon. We do not intend to investigate such detailed models thoroughly, but as an example that further demonstrates the robustness of our results, we also replicate our results with a much more detailed membrane model as first described by Kager et al. [17]. This detailed model contains five different gated ion channels (transient and persistent sodium, delayed rectifier and transient potassium, and NMDA receptor gated currents) and has been used intensively to study spreading depolarizations and seizure-like activity. In fact, one modification is required so that we can replicate our previous results. The detailed model contains an unphysiological so-called ‘fixed leak’ current

$$I_{leak,f} = g_{leak,f} \cdot (V + 70) \quad (35)$$

that has a fixed reversal potential of  $-70$  mV and no associated ion species. This current only enters the rate equation for the membrane potential  $V$  and thereby implies that  $V = -70$  mV is a necessary fixed point condition. In other words, the type of depolarized fixed point that we have found in the simpler model is ruled out by this current. If we, however, replace this unphysical

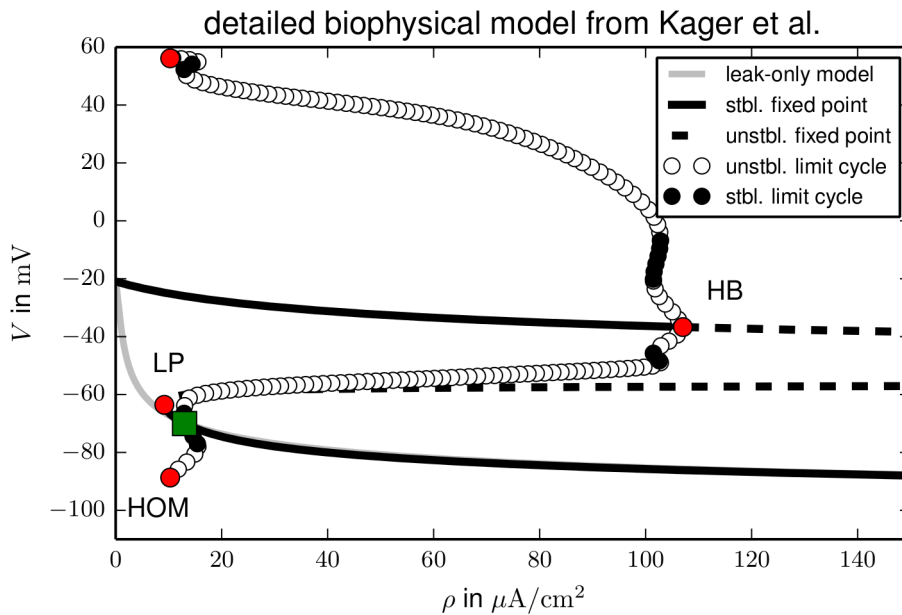


**Figure 7. Bifurcation diagram of the fixed points for the Kager et al. model** [17]. The physiological equilibrium is at  $\rho = 13 \mu\text{A}/\text{cm}^2$ , the minimal physiological pump rate is  $\rho = 9.8 \mu\text{A}/\text{cm}^2$ , and the recovery rate is  $\rho = 107 \mu\text{A}/\text{cm}^2$ . The limit cycle emanating from the HB undergoes four saddle–node bifurcations of limit cycles (indicated by the stability changes, but not explicitly labeled) before it disappears in a homoclinic bifurcation (HOM). Like in Fig. 5 the fixed point line for the corresponding leak–only model is shaded. Its value at  $\rho = 0 \mu\text{A}/\text{cm}^2$  indicates the Donnan equilibrium.

doi:10.1371/journal.pcbi.1003551.g007

current with a chloride leak current as in our model (see eqs. (13), (19), (23)) and furthermore neglect the glial buffering model use in Ref [17], we find the same type of bistability as in our model.

The fixed point continuation of this model (for a complete list of rate equations see [17,34]) in Fig. 7 shows that again FES conditions and a physiological state coexist for a large range of pump rates. This model has slightly different leak conductances and equilibrium ion concentrations, and consequently the characteristic pump rates also differ from ours. However, the only important thing to note here is that the recovery pump rate defined by the subcritical Hopf bifurcation of the upper fixed point branch is large compared to the physiological value (marked by the green square), so also in this rather different membrane model recovery from FES due to pump enhancement is practically impossible. The limit cycle continuation also bears a strong similarity to the one in Fig. 2 with the only main difference being that the limit cycles of the detailed model are stable in two narrow parameter regimes (see solid circles in Fig. 7). We remark that the physiologically irrelevant unstable fixed point branches in Fig. 7 do not connect in a saddle–node bifurcation, but saturate for very high pump rates. The occurrence of the same type of bistability in a Hodgkin–Huxley–based ion model and this very detailed one, and also the similarity of the SD trajectories in Fig. 3 to those presented in [17], support the physiological relevance of the minimal ion–based ansatz that we developed and follow in this paper. Moreover, we assume that bistability is an universal feature also for other more detailed membrane model, which are yet more elaborate variants of the model described by Kager et al. [17]. We will hence use the model from Sec. Model for further investigations.

**Variation of membrane surface and extracellular volume fraction.** After the overview of different variants of ion content, ion channels, pumps and current models we finally address the role of the neuron geometry. Therefore we vary the membrane

surface and the extracellular volume fraction in the model from Sec. Model. For the surface variation we introduce the relative surface size parameter  $\chi_A$  and replace  $A_m$  with  $A_m\chi_A$  which implies the replacement (see eq. (20))

$$\gamma \rightarrow \gamma\chi_A$$

wherever  $\gamma$  occurs, i.e., in the ion rate eqs. (18) and (19) and the sodium constraint eq. (29). The extracellular volume fraction, typically denoted as  $f$ , is defined as

$$f := \frac{\omega_e}{\omega_{tot}} \Rightarrow \omega_e = f\omega_{tot} \quad \text{and} \quad \omega_i = (1-f)\omega_{tot},$$

where  $\omega_{tot} = \omega_i + \omega_e$  is the total volume of the system. When  $f$  is varied, the above expressions for  $\omega_{i/e}$  must be inserted in both ion rate eqs. (18) and (19), and in all ion constraint eq. (24)–(26) and (29). The surface parameter  $\chi_A$  is varied from 0.1 to 10,  $f$  is varied from 2% to 50%. The standard values of these parameters are  $\chi_A = 1$  and  $f = 25\%$  and parameters are understood to take these values when they are not varied. We start from the bifurcation diagram of Fig. 2 and perform two–parameter continuations of the detected bifurcations to find out how the membrane surface and the volume ratio change the bistable regime. The  $(\rho, \chi_A)$ – and  $(\rho, f)$ –continuation curves are shown in the left and right plot of Fig. 8.

We see that the  $\chi_A$  variation has hardly any effect on the bifurcation values of  $\rho$ . This can be understood from the structure of the model. The fixed point curve is defined by setting the rate eqs. (2), (18), (19), (23) to zero and the constraint eqs. (15), (16), (24)–(26) and (29). When  $\chi_A$  is varied the only modification to these conditions is in eq. (29) (sodium constraint). But this modification is of order  $\mathcal{O}(10^{-5})$  and does practically not affect the shape of the fixed point curve, so the limit point bifurcations

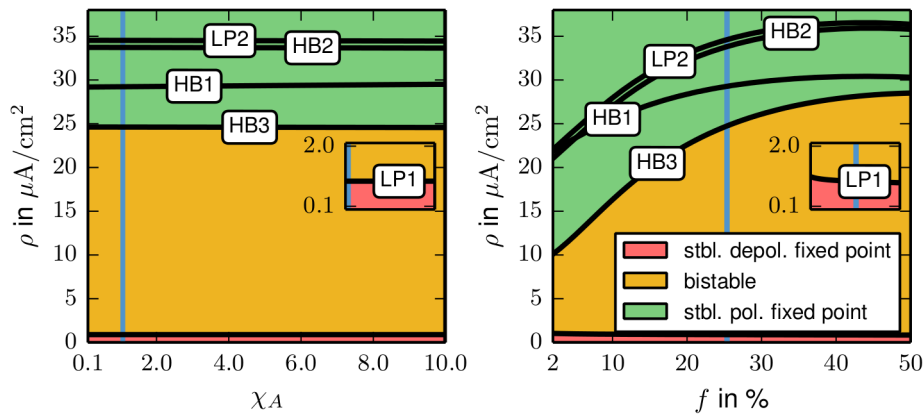


**Figure 8. Two-parameter continuations of the fixed point bifurcations of Fig. 2.** In the left plot the dimensionless surface size parameter  $\chi_A$  is varied, in the right plot the extracellular volume fraction  $f$  is changed. The insets show the LP1 curves that mark the minimal physiological pump rate. The pump rates for which the system is bistable range from the LP1 to the HB3. The HB3 pump rate is required to repolarize a neuron that is in the depolarized equilibrium. The parameter  $\chi_A$  (left plot plus inset) almost does not change the stability of the system, but  $f$  (right plot) reduces the recovery pump rate significantly. The inset shows that the minimal physiological pump rate is much less affected. In each plot and inset the standard parameter value is indicated by the light-blue vertical line.  
doi:10.1371/journal.pcbi.1003551.g008

LP1 and LP2 are almost not changed. Hopf bifurcation could be shifted, but a rescaling of the (initial and dynamical) ion concentrations by  $\chi_A$  transforms the rate and constraint equations such that  $\chi_A$  only appears in the pump currents. Their derivatives are then multiplied by  $\chi_A$ , but for all HBs the pumps are saturated and hence  $\chi_A$  does not contribute to the Jacobian. The variation of  $f$ , however, does change the width (with respect to  $\rho$ ) and the threshold values of the bistable regime. A small value of  $f$  (corresponding to a small extracellular space) reduces the recovery pump rate, and also increases the minimal physiological pump rate. This means that both, depolarization and recovery, are enhanced. However, the minimal physiological pump rate is much less affected than the recovery pump rate, so basically a big cell volume supports recovery from the depolarized state. It is known that in spreading depression (SD), where metastable depolarized states that resemble the energy-starved fixed point of our model occur, the osmotic imbalance of ICS and ECS ion concentrations leads to a water influx that makes the cells swell. Our analysis shows that such a process helps the neuron to return to its physiological equilibrium. Extracellular volume fractions of down to 4% are reported in SD, but even for such extreme volume fractions the required recovery pump rate is too high for pump driven recovery of the neuron (see the lowest value for  $\rho_{HB3}$  in the right plot of Fig. 8). We remark that the bifurcation curves in Fig. 8 do not saturate for  $f > 50\%$ , but, except from the LP1-curve that remains very low, bend down, probably due to an approximate symmetry of ICS and ECS ion concentration dynamics. In summary also the analysis of different cell geometries confirms that ion homeostasis cannot be provided by  $\text{Na}^+/\text{K}^+$  pumps alone. For example, in computational models of dynamically changing pump rates due to oxygen consumption maximal rates of twice the physiological values are considered [22].

## Discussion

Computational neuroscience complements experimental and clinical neuroscience. Simulations help to interpret data and guide a principal understanding of the nervous systems in both health and disease. The HH-formulation of excitability was “so spectacularly successful that, paradoxically, it created an unrealistic expectation for its rapid application elsewhere” as Noble

remarked [9]. While his statement refers to modeling of cardiac cells it certainly holds true also for neurological diseases and brain injury [11,13]. In both fields, the incorporation of the  $\text{Na}^+/\text{K}^+$  pump in the original excitability paradigm formulated by Hodgkin and Huxley is of major importance. The fundamental structure of such models has to our knowledge not been exploited in neuroscience beyond merely modulating spiking in epileptiform activity [23,24] or in models that have energy-starved states [17–22,32] yet without investigating the fundamental bifurcation structure.

As we stressed in the introduction, this extension of the original HH model enforces a physical or rather thermodynamical perspective, which was, of course, the starting point of Hodgkin and Huxley, too. For instance, we also considered the Goldman–Hodgkin–Katz (GHK) current equation which is derived from the constant field assumption applied to the Nernst–Planck equation of electrodiffusion. Electroneutrality is important to consider, as can be seen by the indirect insertion of impermeable counter anions only reflected by observing a thermodynamic Donnan equilibrium. Furthermore, a thermodynamic description of osmotic pressure (which would require a direct insertion of a concentration  $A^{n-}$  of a counter anion with valence  $n$ ) and corresponding changes in cell volume can be included.

There are further physical mechanisms that may alter the dynamics in biophysical ion-based models. At the same time, we have to avoid “an excruciating abundance of detail in some aspects, whilst other important facets [...] can only be guessed” [41], like using various new currents but guessing the correct value of the valence  $n$  of an impermeable counter anion. For this reason, we decided to use the original ion currents from the HH model. The comparison of our results to a physiologically more realistic and much more detailed membrane model in Fig. 7 support the assumption that the basic structure will not be changed by just adding or modifying gating. This question has also been addressed experimentally and in simulations by showing that only the simultaneous blockade of all known major cation inward currents did prevent hypoxia-induced depolarization with FES [17,42]. In the model [17], five different  $\text{Na}^+$  currents were investigated. Of course, to apply our model to a particular pathological condition, like migraine which is a channelopathy [43,44] (disease caused by modified gating), these details will become important. This can



easily be incorporated in future investigations. Moreover, note that changes in cell volume, which are very important in brain injuries, are in this study only treated by varying it as a parameter.

Our bifurcation analysis shows that a whole class of minimal ion-based models is bistable for a large range of pump rates ( $\rho_{LPI} < \rho < \rho_{HB3}$ ). Bistable dynamics was suggested by Hodgkin to explain spreading depression [11,12], and a corresponding model has been investigated mathematically by Huxley but never been published (cf. Ref. [45]). Dahlem and Müller suggested to extend this ad hoc approach, i.e., a single so-called activator variable with a bistable cubic rate function, by including an inhibitory mechanism in form of an inhibitor species with a linear rate function coupled to the activator [45]. This, of course, leads to the well known FitzHugh–Nagumo paradigm of excitability type II [46,47], that is, excitability caused by a Hopf bifurcation [48], but should not be mistaken as a modification of conductance-based excitability in form of HH-type model in the ‘first generation’ and the interpretation as an equivalent electrical circuit. FitzHugh used his equation in this way, he investigated a long plateau as seen in cardiac action potentials. Dahlem and Müller suggested to use the same mathematical structure of an activator–inhibitor type model [45] to describe a fundamental new physiological mechanism of ionic excitability that originates from bistable ion dynamics. Our current results provide the missing link between this ad hoc activator–inhibitor approach, which has been widely used in migraine and stroke pathophysiology [45,49–58], and biophysical plausible models. The major result from this link is the new interpretation of the physiological origin of the proposed inhibitory variable [45]. We wrongly interpreted it as being related to the pump rate [49,51,53,57].

As our ion-based model shows bistable dynamics, we see it as essentially capturing the activator dynamics of an excitable system and briefly show in Figs. 2 and 3 that it can be transformed into such a system by the introduction of a inhibitory process. Vice versa, excitable systems can be reduced to bistable dynamics by singular perturbation methods. Such reductions are referred to as a threshold reduction. From this perspective our model can be interpreted as the threshold reduction of an excitable system, and we conclude that without contact to an ion bath, physically

realistic ion-based models miss an important inhibitory mechanism. Our analysis shows that unlike what we thought before [49,51,53,57], ion pumps alone are insufficient. If the pump rate is temporarily decreased to less than the minimal physiological rate, the neuron depolarizes, and normal pump activity does not suffice to recover the physiological state. Depending on the particular model the required recovery pump rates range from three times up to more than 30 times the original value. These high values suggest that also more detailed pump models that, for example, include the coupling of the maximal pump rate to oxygen or glucose [22] will not resolve this bistability.

It can, however, also be seen that a regulation term for the extracellular ion concentrations that mimics glial buffering and coupling to the vasculature will allow only monostability. An additional diffusive coupling to a bath value in the extracellular rate equations forces all such buffered extracellular species to assume the respective bath concentrations. There are no two points on the solution branch that share the same extracellular potassium concentrations (see Fig. 4). Hence one fixed point is selected, the other state becomes unstable. We consequently suspect that coupling to some bath (glia/vasculature) plays a crucial role in maintaining ion homeostasis and our results from Figs. 3 and 4 confirm that an ion-based model including such coupling will recover from superthreshold perturbations by a large excursion in phase space that is characterized by long transient free energy–starvation.

## Acknowledgments

The authors are grateful for discussions with Jens Dreier on spreading depolarizations, scientific guidance by Michael Guevara on ion-based models in myocytes, and Steven J. Schiff and Nancy Kopell, for various helpful discussions.

## Author Contributions

Conceived and designed the experiments: MAD NH. Performed the experiments: NH MAD. Analyzed the data: NH MAD ES. Contributed reagents/materials/analysis tools: NH MAD. Wrote the paper: NH MAD ES.

## References

- Hodgkin AL, Huxley AF (1952) A quantitative description of membrane current and its application to conduction and excitation in nerve. *J Physiol* 117: 500.
- Beilby MJ, Coster HGL (1979) The action potential in *chara corallina* III.\* the Hodgkin-Huxley parameters for the plasmalemma. *Funct Plant Biol* 6: 337–353.
- Ebihara L, Johnson E (1980) Fast sodium current in cardiac muscle. A quantitative description. *Biophys J* 32: 779–790.
- Chay TR, Keizer J (1983) Minimal model for membrane oscillations in the pancreatic beta-cell. *Biophys J* 42: 181–190.
- Atwater I, Dawson CM, Scott A, Eddlestone G, Rojas E (1980) The nature of the oscillatory behaviour in electrical activity from pancreatic beta-cell. *Horm Metab Res Suppl* 10: 100–107.
- Cha CY, Nakamura Y, Himeno Y, Wang J, Fujimoto S, et al. (2011) Ionic mechanisms and  $Ca^{2+}$  dynamics underlying the glucose response of pancreatic  $\beta$  cells: a simulation study. *J Gen Physiol* 138: 21–37.
- DiFrancesco D, Noble D (1985) A model of cardiac electrical activity incorporating ionic pumps and concentration changes. *Phil Trans R Soc B* 307: 353–398.
- Dokos S, Celler B, Lovell N (1993) Modification of diFrancesco-noble equations to simulate the effects of vagal stimulation on in vivo mammalian sinoatrial node electrical activity. *Annals of biomedical engineering* 21: 321–335.
- Noble D, Rudy Y (2001) Models of cardiac ventricular action potentials: iterative interaction between experiment and simulation. *Phil Trans R Soc A* 359: 1127–1142.
- Arce H, Xu A, González H, Guevara MR (2000) Alternans and higher-order rhythms in an ionic model of a sheet of ischemic ventricular muscle. *Chaos: An Interdisciplinary Journal of Nonlinear Science* 10: 411–426.
- Dreier JP (2011) The role of spreading depression, spreading depolarization and spreading ischemia in neurological disease. *Nat Med* 17: 439–447.
- Charles AC, Baca SM (2013) Cortical spreading depression and migraine. *Nat Rev Neurol* 637–44. doi: 10.1038/nrneurol.2013.192.
- Dreier JP, Isele TM, Reiffurth C, Kirov SA, Dahlem MA, et al. (2013) Is spreading depolarization characterized by an abrupt, massive release of Gibbs free energy from the human brain cortex? *Neuroscientist* 19: 25–42.
- Varghese A, Sell GR (1997) A conservation principle and its effect on the formulation of Na-Ca exchanger current in cardiac cells. *J Theor Biol* 189: 33–40.
- Endresen L, Hall K, Høye J, Myrheim J (2000) A theory for the membrane potential of living cells. *Eur Biophys J* 29: 90–103.
- Cha CY, Himeno Y, Shimayoshi T, Amano A, Noma A (2009) A novel method to quantify contribution of channels and transporters to membrane potential dynamics. *Biophys J* 97: 3086–3094.
- Kager H, Wadman WJ, Somjen GG (2000) Simulated seizures and spreading depression in a neuron model incorporating interstitial space and ion concentrations. *J Neurophysiol* 84: 495–512.
- Shapiro BE (2001) Osmotic forces and gap junctions in spreading depression: a computational model. *J Comput Neurosci* 10: 99–120.
- Miura RM, Huang H, Wylie JJ (2007) Cortical spreading depression: An enigma. *Eur Phys J Spec Top* 147: 287–302.
- Somjen GG, Kager H, Wadman WJ (2008) Computer simulations of neuronal-glia interactions mediated by ion flux. *J Comput Neurosci* 25: 349–365.
- Zandt BJ, ten Haken B, van Dijk JG, van Putten MJ (2011) Neural dynamics during anoxia and the “wave of death”. *PLoS ONE* 6: e22127.
- Chang JC, Brennan KC, He D, Huang H, Miura RM, et al. (2013) A mathematical model of the metabolic and perfusion effects on cortical spreading depression. *PLoS ONE* 8: e70469.
- Cressman Jr JR, Ullah G, Ziburkus J, Schiff SJ, Barreto E (2009) The influence of sodium and potassium dynamics on excitability, seizures, and the stability of persistent states: I. single neuron dynamics. *J Comput Neurosci* 26: 159–170.
- Barreto E, Cressman JR (2010) Ion concentration dynamics as a mechanism for neural bursting. *J Biol Phys* 37: 361–373.

25. Yu N, Morris CE, Joos B, Longtin A (2012) Spontaneous excitation patterns computed for axons with injury-like impairments of sodium channels and Na/K pumps. *PLoS Comput Biol* 8: e1002664.
26. Boucher PA, Joos B, Morris CE (2012) Coupled left-shift of Nav channels: modeling the Na-loading and dysfunctional excitability of damaged axons. *J Comp Neurosci*: 1–19.
27. Fröhlich F, Bazhenov M, Iragui-Madoz V, Sejnowski TJ (2008) Potassium Dynamics in the Epileptic Cortex: New Insights on an Old Topic. *Neuroscientist* 14: 422–433.
28. Fröhlich F, Bazhenov M (2006) Coexistence of tonic firing and bursting in cortical neurons. *Phys Rev E* 74: 031922.
29. Bazhenov M, Timofeev I, Steriade M, Sejnowski TJ (2004) Potassium model for slow (2–3 Hz) in vivo neocortical paroxysmal oscillations. *J Neurophysiol* 92: 1116–1132.
30. Aihara K, Matsumoto G (1983) Two stable steady states in the Hodgkin-Huxley axons. *Biophys J* 41: 87–89.
31. Hahn PJ, Durand DM (2001) Bistability dynamics in simulations of neural activity in high-extracellular-potassium conditions. *J Comput Neurosci* 11: 5–18.
32. Florence G, Dahlem MA, Almeida ACG, Bassani JWM, Kurths J (2009) The role of extracellular potassium dynamics in the different stages of ictal bursting and spreading depression: A computational study. *J Theor Biol* 258: 219.
33. Cressman Jr JR, Ullah G, Ziburkus J, Schiff SJ, Barreto E (2009) The influence of sodium and potassium dynamics on excitability, seizures, and the stability of persistent states: I. single neuron dynamics. *J Comput Neurosci* 26: 159–170.
34. Yao W, Huang H, Miura RM (2011) A continuum neural model for the instigation and propagation of cortical spreading depression. *Bull Math Biol* 73: 2773–2790.
35. Rinzel J, Ermentrout GB (1989) Analysis of neural excitability and oscillations. In: Koch C, Segev I, editors, *Methods in neuronal modeling*, Cambridge, MA: MIT Press, pp. 251–291.
36. Ermentrout GB, Terman D (2010) *Mathematical Foundations of Neuroscience*. Springer.
37. Zamecnik J, Homola A, Cicanic M, Kuncova K, Marusic P, et al. (2012) The extracellular matrix and diffusion barriers in focal cortical dysplasias. *Eur J Neurosci* 36: 2017–2024.
38. Xie L, Kang H, Xu Q, Chen MJ, Liao Y, et al. (2013) Sleep drives metabolite clearance from the adult brain. *Science* 342: 373–377.
39. Doedel EJ, Oldeman BE (2009) *Auto-07P: Continuation and bifurcation software for ordinary differential equations*. Concordia University, Montreal, Canada.
40. Kuznetsov YA (1995) *Elements of Applied Bifurcation Theory*. New York: Springer.
41. May RM (2004) Uses and abuses of mathematics in biology. *Science* 303: 790–793.
42. Muller M, Somjen GG (1998) Inhibition of major cationic inward currents prevents spreading depression-like hypoxic depolarization in rat hippocampal tissue slices. *Brain Res* 812: 1–13.
43. Silberstein S, Dodick D (2013) *Migraine Genetics - A Review: Part I. Headache* 53: 1207–17.
44. Silberstein SD, Dodick DW (2013) *Migraine Genetics: Part II. Headache* 53: 1218–29. doi: 10.1111/head.12169.
45. Dahlem MA, Müller SC (2004) Reaction-diffusion waves in neuronal tissue and the window of cortical excitability. *Ann Phys* 13: 442–449.
46. FitzHugh R (1961) Impulses and physiological states in theoretical models of nerve membrane. *Biophys J* 1: 445–466.
47. Nagumo J, Arimoto S, Yoshizawa S (1962) An active pulse transmission line simulating nerve axon. *Proc IRE* 50: 2061–2070.
48. Ermentrout GB (1998) Neural networks as spatio-temporal pattern-forming systems. *Rep Prog Phys* 61: 353–430.
49. Dahlem MA, Schneider FM, Schöll E (2008) Efficient control of transient wave forms to prevent spreading depolarizations. *J Theo Biol* 251: 202–209.
50. Dahlem MA, Schneider FM, Schöll E (2008) Failure of feedback as a putative common mechanism of spreading depolarizations in migraine and stroke. *Chaos* 18: 026110.
51. Dahlem MA, Hadjikhani N (2009) Migraine aura: retracting particle-like waves in weakly susceptible cortex. *PLoS ONE* 4: e5007.
52. Postnov DE, Müller F, Schuppner RB, Schimansky-Geier L (2009) Dynamical structures in binary media of potassium-driven neurons. *Phys Rev E* 80: 031921.
53. Dahlem MA, Graf R, Strong AJ, Dreier JP, Dahlem YA, et al. (2010) Two-dimensional wave patterns of spreading depolarization: retracting, re-entrant, and stationary waves. *Physica D* 239: 889–903.
54. Schneider FM, Schöll E, Dahlem MA (2009) Controlling the onset of traveling pulses in excitable media by nonlocal spatial coupling and time delayed feedback. *Chaos* 19: 015110.
55. Dahlem MA, Isele TM (2013) Transient localized wave patterns and their application to migraine. *J Math Neurosci* 3: 7.
56. Postnov DE, Postnov DD, Schimansky-Geier L (2012) Self-terminating wave patterns and self-organized pacemakers in a phenomenological model of spreading depression. *Brain Res* 1434: 200–211.
57. Dahlem MA (2013) Migraine generator network and spreading depression dynamics as neuromodulation targets in episodic migraine. *Chaos* 23: 046101.
58. Dahlem MA, Rode S, May A, Fujiwara N, Hirata Y, et al. (2013) Towards dynamical network biomarkers in neuromodulation of episodic migraine. *Transl Neurosci* 4: 282–294.